JOURNAL OF MATERIALS SCIENCE 31 (1996) 1405–1413

Electron spin resonance *in situ* observation of the bending stress process in corundum materials and glasses

R. STOESSER, N. STEINFELDT
Humboldt-University of Berlin, Chemical Institute, Hessische Strasse 1-2, 10115 Berlin, Germany

R. BRENNEIS, M. NOFZ
Federal Institution of Material Science and Testing, Rudower Chaussee 5, 12489 Berlin, Germany

A new combination of three-point bending stress and electron spin resonance (ESR) methods was developed and successfully tested in the field of glassy and ceramic materials. Summarizing the observed phenomena, one can establish the following advantages of such an experimental combination: (i) direct and continuous observation of the material under the action of bending stress up to mechanical destruction of the sample; (ii) optically transparent samples are not necessary, but a further direct combination with optical methods is, in general, possible; (iii) the high sensitivity and selectivity of the ESR method allow the first steps of stress influence on the local geometry to be followed long before the crack appears and fracture takes place, respectively; (iv) local effects are observed on the atomic scale which can be related to the mechanical properties by an appropriate hamiltonian; (v) the reversibility of the effects can easily be proved by a suitable alternating stress/relaxation regime; (vi) variation of further parameters such as temperature or application of tensile stress, is possible.

1. Introduction

Properties governing the function of a material are often derived directly from its overall chemical composition or from structural models. Such models may be developed on the basis of the experimental findings as results of the combined action of local electric and magnetic fields as well as external mechanical forces on materials, respectively. Furthermore, many essential physical and chemical processes do not correspond to the actual specimen as a whole. They often take place in distinct regions of the material, e.g. in the neighbourhood of impurities or dopants, in clusters, at the boundary of phases originally present in the material or even formed in it.

If the knowledge concerning the inner processes is derived only from the macroscopic response to an external mechanical force, it is, in general, difficult to explain the observed effects on a microscopic level. The direct combination of mechanical and spectroscopic methods can help to overcome this problem and yield new insight into the local properties of a solid material.

Dealing with high-pressure studies of hard and other inorganic materials [1–5] we successfully built up a combined equipment consisting of a conventional three-point bending stress arrangement with a cw-ESR (electron spin resonance) spectrometer (9 GHz). To our knowledge this paper is the first publication concerning this kind of direct experimental combination. There is no report available in the literature related to the *in situ* combination of these two methods for the application in material science.

2. Experimental procedure

The three-point bending stress method was used for the experiments because of its simplicity and widespread use. The required geometry of the sample and the mechanical parameters, i.e. the not too high maximal moment of tension, which is effective at the middle part of the sample (Fig. 1a, e), provide good prerequisites for a direct combination of this mechanical method with ESR spectroscopy. The bending stress can, after developing a suitable equipment, directly be applied in the cavity of an ESR X-band spectrometer (E4, Fa. Varian, USA). The experimental arrangement shown in Fig. 1 was used for the investigations presented here. As shown in Fig. 1a and b, rod-like samples (cut corundum materials [6, 7] of $63 \times 4 \times 3$ mm^3 as well as glassy rods of 5 mm diameter and 63 mm length) were supported twice over a distance of 50 mm. A quartz rod of 4 mm diameter (Fig. 1e) served as a transfer of the force from the calibrated spring

0022–2461

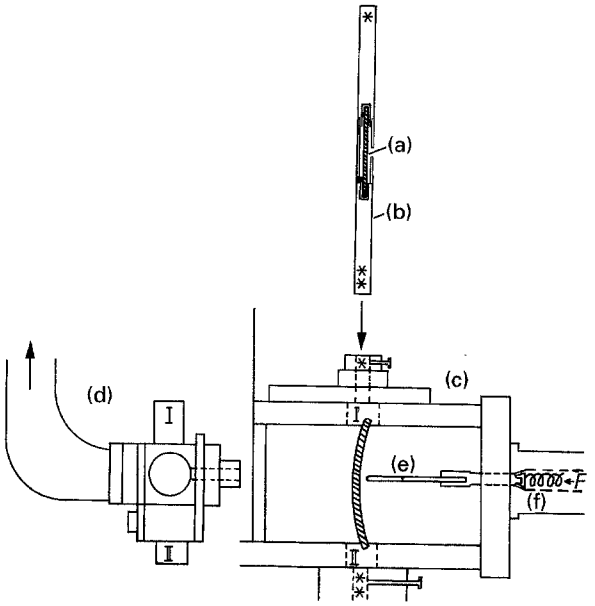

Figure 1 Schematic representation of the apparatus for the ESR *in situ* bending stress measurements: a, sample; b, sample holder with the two-point sample support; c, non-magnetic box for the consolidation of d and e; d, cavity of the X-band spectrometer (Varian E4); e, quartz rod for the transmission of the mechanical force, F, caused by the calibrated spring, f.

(Fig. 1f) to the central point of the sample. The bending stress, σ_B, was calculated on the basis of the formula

$$\sigma_B = 1.5\, F\, (h^2\, b)^{-1} \qquad (1)$$

where h and b are length and breadth of the specimen, respectively, l is the distance between the outer supports and F is the force caused by the spring.

A Teflon-made tube enveloping the bent sample protects the ESR cavity in the case of the mechanical destruction of the specimen. All materials contributing finally to the electric load of the cavity were carefully selected with respect to their dielectric properties as well as their geometries, in such a manner that the quality factor of the cavity was only little changed. All other parts of the bending stress equipment were made from non-magnetic materials such as brass (Fig. 1b, c).

Further ESR experiments performed at 4 K were done with the help of a flow cryostat (APD cryogenics, USA) combined with the X-band spectrometer ERS300 (Zentrum für wissenschaftlichen Gerätebau, Berlin-Adlershof, Germany).

3. Results and discussion

3.1. Fusion-cast corundum materials

First, the results obtained for fusion-cast corundum materials will be discussed. As we were able to show [6], these materials contain rather different iron species. Their oxidation state, concentration and localization in an actual sample depend on the melting conditions as well as on the post-melting processing. Some of the Fe^{3+} ions substitute the Al^{3+} ions in the corundum lattice and can be used as a spin probe, reporting even small structural changes of the main phase of the composite solid. A typical ESR spectrum

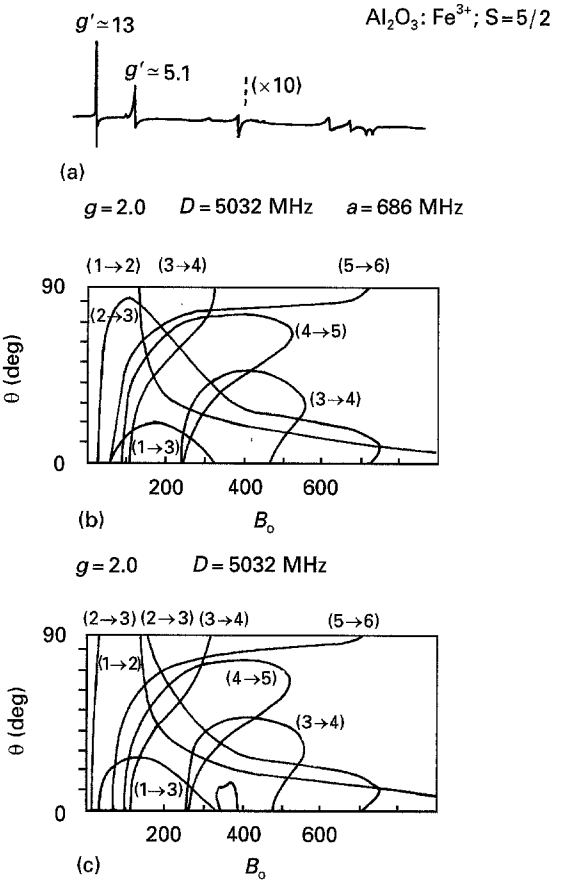

Figure 2 ESR of Fe^{3+} ions substituting Al^{3+} in α-Al_2O_3. (a) Experimental X-band spectrum (77 K); (b) computed angular dependence of the transitions between the spin states using the zero-field splitting paramater, D, and the cubic splitting constant a; (c) computed angular dependence of the transitions between the spin states using the zero-field splitting paramater, D, but neglecting the cubic splitting constant, a.

of these ions with a ^6S ground state is shown in Fig. 2a. For assignment of the resonances and an understanding of the relations between pressure-induced structural and spectroscopic changes, a simulation of the powder spectra is necessary (see also [8]). The simulations performed here were based on the parameters of a spin hamiltonian derived from the corresponding single-crystal ESR measurements. Not only the zero-field splitting (zfs; $|D| = 0.1483\ cm^{-1}$) but also the parameters of the fourth-order $|(a-F)| = 0.048\ cm^{-1}$ had to be taken into account (cf. Fig. 2 and Figs 7 and 8 below). Additionally, the patterns of the experimental spectra exhibit specific powder effects caused by surface, internal tensions and disorder effects. Strain effects, especially, contribute to the distribution of the parameters of the spin hamiltonian for $S = 5/2$. Thus, the single-crystal ESR parameters can only be used as a starting approximation but the full simulation must be carried out with respect to the effects inherently present in the powder or induced by external forces, respectively. Using this procedure all ESR signals of the Fe^{3+} species in the glassy phase containing corundum compact materials could be assigned: in addition to the Fe^{3+} ions on Al^{3+} sites of the corundum lattice mentioned above, there is evidence for Fe^{3+} (i) substituting Al^{3+} in the glassy network ($g' \simeq 4.3$; Fig. 3b), and (ii) at inner and

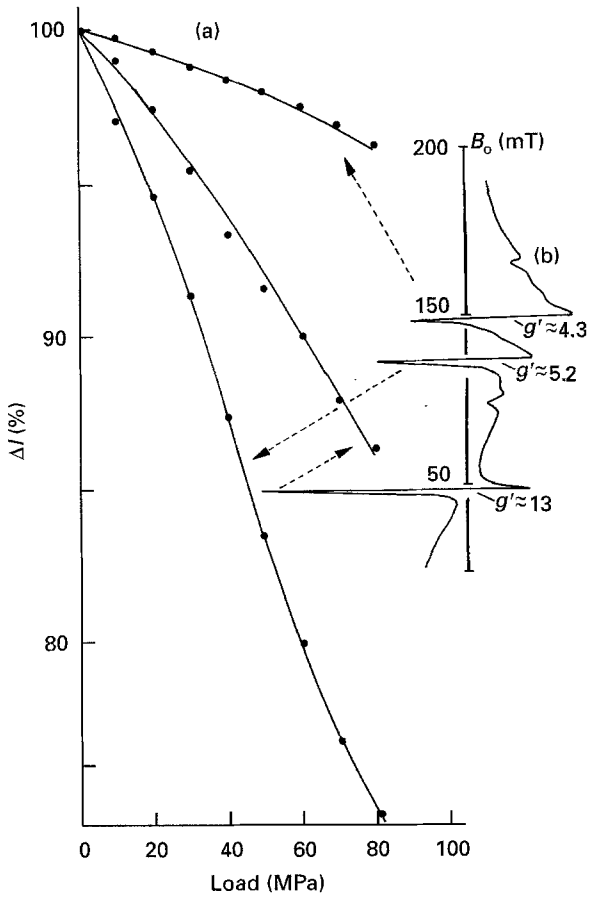

Figure 3 Application of bending stress to a fusion-cast corundum sample containing 20 vol % glassy phase: (a) the change of the ESR intensity, ΔI, of the iron species incorporated in the corundum ($g' \simeq 13$ and 5.3) and glassy phases ($g' \simeq 4.3$) as a function of the applied bending load; (b) the corresponding experimental ESR spectrum.

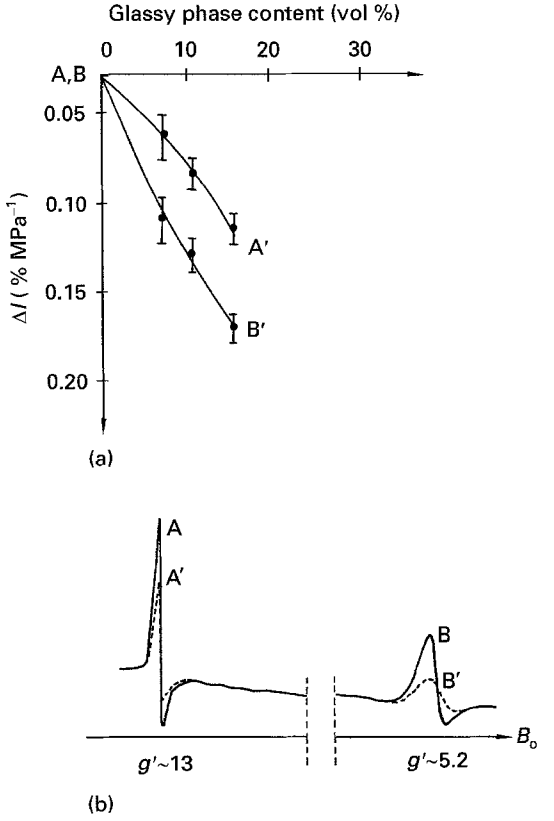

Figure 4 Influence of the glassy phase content on the ESR bending stress response. (a) ΔI is the decrease of the ESR intensity per MPa load. The bars mark the scatter of the points using 5–10 different samples; (b) spectral changes induced by bending stress.

outer surfaces of this heterogeneous system also contributing to the $\mathbf{g}' \simeq 4.3$ region. (The spectral contribution of such Fe^{3+} species could be evinced by the ESR spectra of fine dispersed Al_2O_3 particles prepared from AlN by high-temperature oxidation in an oxygen atmosphere [9, 14].) Furthermore, exchange-coupled paramagnetic species, as well as traces of Cr^{3+} ions, could be indicated in the low-field region [7]. FeO_x species precipitated at the grain boundaries ($3.5 > g' > 2.3$) sensitively react on external forces by changing their resonance field positions and intensities [9, 10].

The response of the substitutional Fe^{3+} ions to bending stress in the matrix leads to directly observable ESR intensity effects which are accompanied by small shifts of the corresponding transitions (Figs 3 and 4). These effects could be measured with sufficient accuracy because they result in each case from one and the same sample under the same experimental and spectrometer conditions. The values for each point used for the construction of the curves in Figs 3 and 4 represent averages of measurements performed on five to ten different samples, taken from the same region of the bulk of the fusion-cast material.

It is remarkable that the observed decrease of the ESR intensities is a result of a slightly non-linear response. This implies that a superposition of elastic and irreversible deformations of the material caused by the mechanical perturbations have to be taken into account. This was demonstrated by further experiments. Fig. 5 displays the dependence of the ESR signal intensities caused by Fe^{3+} ions on Al^{3+} sites in the corundum lattice as a function of the bending stress applied. All curves of Fig. 5 reflect linear elastic behaviour of the material for not too large loads. A larger contribution of inelastic and, to a greater extent, irreversible processes, results above a load of 40 MPa (not shown here). In many cases, immediately after passing the last observable measuring point, the fracture of the material took place without further enlarging the load. Thus, the inner tensions of the material exceed the border of the binding forces between the structural units and the material relaxes by fracture. In contrast to that, in a few other observed cases, the material was broken during the ESR experiment but the spectral response indicated elastic behaviour up to this point. In other words, there is a load region in which the loading/unloading (relaxing) processes could be carried out reversibly. Each loading and relaxation period was limited, in the experiments discussed here, to 16 min. As Fig. 5 shows for the loads < 40 MPa, the ESR intensities return exactly to their starting values during the relaxation period.

Only small changes were observed for the signals at $\mathbf{g}' \simeq 4.3$ caused essentially by Fe^{3+} ions in the glassy phase together with a small contribution of Fe^{3+} located at the surface.

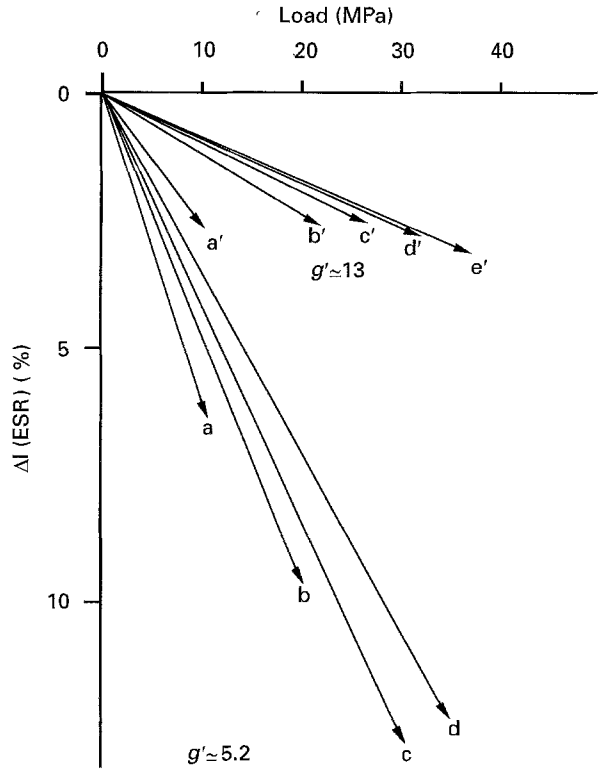

Figure 5 Results of alternating (time interval for loading and relieving of stress = 16 min) bending stress experiments: decrease of the ESR intensity as a function of the load applied repeatedly. Every loading process starts with an external load of zero and runs to a, b, c, d and a', b', c', d', respectively, and after 16 min back to zero.

In the bending stress range investigated here, the glassy phase as a constituent of the corundum material remains only sightly affected (Fig. 3). But the ESR method is sensitive enough to detect the small structural changes induced by bending stress experiments in pure glassy materials (see below, Figs 9, 10). In general, this corresponds to pressure experiments on glasses yielding small effects on the Fe^{3+} species incorporated in the glass only in the GPa range [3].

As known from the macroscopically determined mechanical properties of the corundum material discussed here [6, 11], the resistance against the bending stress increases with increasing content of the glassy phase (1.5–33 vol % fusion-cast corundum material) having the composition 11.0 Na_2O, 30.5 Al_2O_3, 58.5 SiO_2 (wt %). This result was confirmed by the ESR studies presented here. The glassy phase not only fills the cavities in the bulk material but also forms binding forces in the interphase layer between the glassy and crystalline phases, respectively.

The application of bending stress to corundum materials and simultaneous observation of the effects by ESR *in situ* features some interesting phenomena: (i) the findings of the commonly used macroscopic bending stress experiment, in the stress range 20–100 MPa (see Figs 3–5) could be reproduced. The Fe^{3+} ions substituting Al^{3+} ions (Fe^{3+}: Al^{3+} = 1:6000) appear to be suitable probes for the indication of local structural changes in the lattice which cannot be observed by other methods; (ii) in contrast to uniaxial pressure experiments performed with the same material [5, 9], essential changes of the intensities of the ESR transitions were observed. Uniaxial pressure experiments yield both line shift as well as intensity (i.e. line-width) effects. The intensity changes observed here by ESR range between 1% and approximately 10%. In comparison to macroscopic measurements [12], yielding an elasticity range of ~1% to 2% of the corundum material, the observed ESR effects appear to be quite large. This difference is due to the very sensitive reaction of the ESR intensity to even small structural changes. This can be explained as follows: one can assume that the whole concentration of the Fe^{3+} species remains unchanged during the bending stress experiment. Therefore, the area A covered by the ESR transitions should also be constant and the simplified relation between the intensity, I_i, the line width ΔB_i of the transition i, and A can be used to discuss the observed effects: $A_i = I_i \Delta B_i^2$. Thus, only small changes of ΔB_i cause a distinct change in the intensity. The line broadening caused by the (external) bending stress superimposes the intrinsic effects of broadening (e.g. due to internal tensions and is characterized by more or less symmetric distributions ($I_i = I_i'(B_i)$) of the ESR fine structure parameters. A more quantitative estimation based on spectra simulations yields a distribution of $\pm 6 \times 10^{-2}|D|$. This distribution of the zero-field splitting is caused on a microscopic scale by stress-induced small elongations as well as compressions of the Fe^{3+} coordination polyhedra in the corundum lattice. In addition to this, the tension causes small changes of the orientations of the individual magnetic axes of the paramagnetic centres with respect to the external magnetic induction, B_0. Both effects contribute to the distribution of the parameters of the static spin hamiltonian.

From the simulation of the ESR spectra one can deduce to what extent the various transitions belonging to different spin states $\pm 1/2$, $\pm 3/2$ and $\pm 5/2$ contribute to the individual peaks of the powder spectra (see Fig. 2). This provides the basis for the elucidation of the observed distinct reaction of the individual ESR signals to bending stress. The unexpected effect that the narrow signal at $g' \simeq 13$ (Fig. 3) is less influenced by the bending stress than that at $g' \simeq 5.1$ has its origin in an extended superposition of contributions of different and stronger angular-dependent transitions to the last one (Fig. 2b, c). Since spin states with higher values of the spin quantum number m_s (e.g. $m_s = \pm 3/2, \pm 5/2$) experience stronger interactions with B_0 as well as with the lattice, a more pronounced angular dependence of the signals (Fig. 2b, c) results. The transitions with the largest angular dependence essentially decide the response to the stress applied. This relation holds, in a modified manner, also for uniaxial pressure experiments even if pressure gradients are present [10, 13]. The different natures of the transitions at $g' \simeq 13$ and 5.2 and the resulting different effective couplings to the lattice are also demonstrated in Fig. 6. A distinct spin-relaxation behaviour for the two discussed transitions results. The dependence on the microwave power applied of the ESR response in and out of phase with the field modulation (100 kHz), is characteristic for the two different sets of transitions at $g' \simeq 5.2$ and 13.

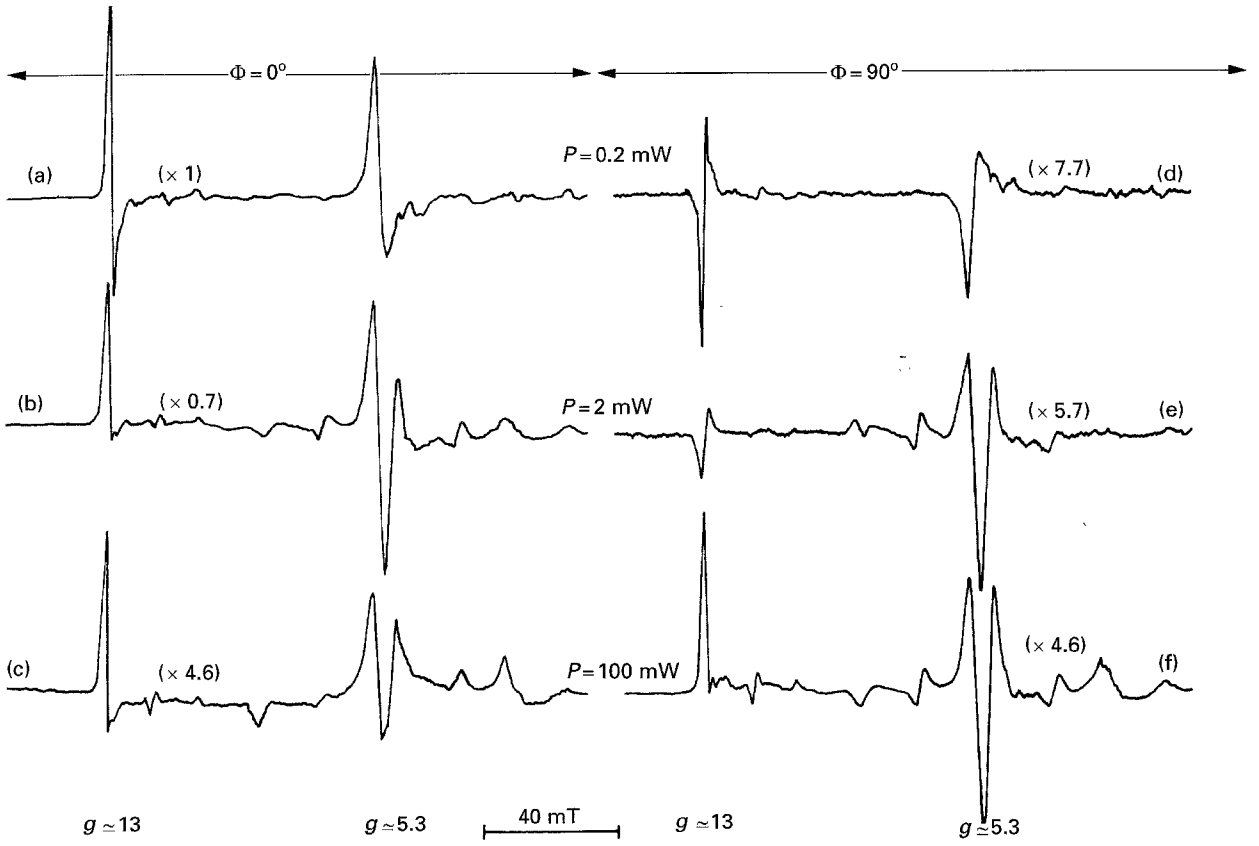

Figure 6 Microwave saturation behaviour of Fe^{3+} ions in α-Al_2O_3 at 4 K. (a–c) In-phase ESR signal of the low-field part of the spectrum at the variation of microwave power over three decades of magnitude; (d–f) the corresponding out-of-phase signals.

For a microscopic picture, it is of interest how the different parameters of the spin hamiltonian contribute to the line shift and intensity effects. Figs 7 and 8 give, by systematic variation of the constants D, a and F, an impression of that dependence. While the positions of the transitions $1 \rightarrow 2$ and $5 \rightarrow 6$ are only slightly affected by the variation of the cubic splitting constants a and F, respectively, the influence of D (and therefore of a D distribution) also is clearly shown in Fig. 7c. In contrast, the ratio of the intensities of the two resonances as observed by the bending stress measurement is more influenced by a and F than by $|D|$ (see Fig. 8).

As shown by the ESR *in situ* uniaxial pressure and bending stress investigations of the compact glassy phase containing corundum materials, these combined experiments gave no direct information concerning the mechanical influence on the incorporated glassy phase. Thus, the stress influence on the Fe^{3+} ions in the glassy compartments of the material is rather small. But, as mentioned above, the glassy phase present in the systems enlarges the mechanical stability of those materials. The main effect here results from the decrease of porosity. Specimens of fusion-cast polycrystalline corundum materials which contain only traces of a glassy phase are characterized by a high degree of porosity and, consequently, the mechanical strength is much less than that of the single-crystalline or glassy-phase containing materials. This difference is caused at last by macroscopic reasons and can be related to the thermal properties of corundum: (i) large volume shrinkage during crystallization from the melt, and (ii) further contraction processes during cooling the solid material to room temperature. The last effect could also be monitored *in situ* by the changes of the Fe^{3+} ESR fine structure in the temperature range $3 \leqslant T \leqslant 1073$ K. Because the zero-field splitting is increased by distortions when lowering the temperature, the low-field transition ($g' \simeq 13$) exhibits a distinct high-field shift. On the contrary, a low-field shift results at higher temperatures, indicating a lowering of the zfs parameter, D, by thermally induced averaging of the distortions of the $[FeO_6]$ polyhedra. This statement could only be given on the basis of the simulation of the ESR spectra, yielding, for example, an increase of D of 5.3% for the temperature change from 300 K to 77 K.

3.2. Glasses

The large resistance of glasses against uniaxial and isostatic pressure at room temperature is well known. Thus, when applying pressure, only small deformations of the glassy network result and, as a consequence, the coordination polyhedra of the incorporated paramagnetic ions remain only slightly changed [6]. One of the specific advantages of the combined spectroscopic and bending stress measurements to glasses rests in the fact that the network reacts much more sensitively to the tensions formed in the material than to the pressure applied. During the application of tensile stress, locally some binding forces are diminished and certain chemical bonds become

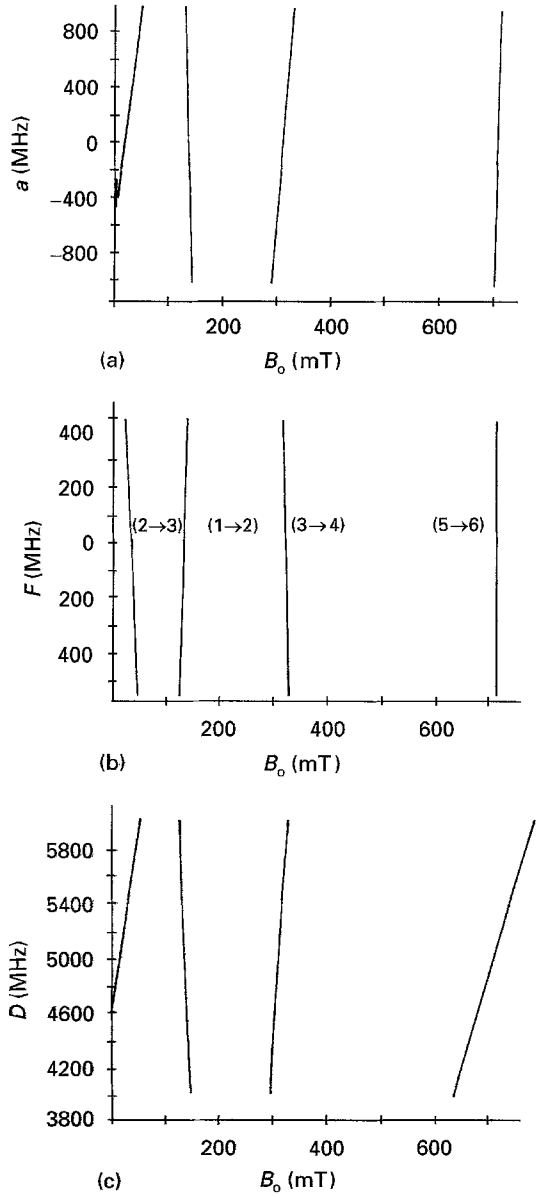

Figure 7 Positions of the resonance fields computed for Fe^{3+} ($^6S_{5/2}$ ground state) in a powder with a spin hamiltonian for trigonal symmetry (see also [8]) with $g = 2.0026$, $|D| = 5130$ MHz, $a = 700$ MHz, $F = -500$ MHz (these parameters correspond to the simulation of Fe^{3+} ions containing corundum material measured by ESR at 2.4 K). (a) Variation of the line positions with the cubic splitting constant a for $D = 5000$ MHz and $F = 0$; (b) as (a) at the variation of F with $D = 5000$ MHz and $a = 600$ MHz; (c) variation of $|D|$ with $a = F = 0$.

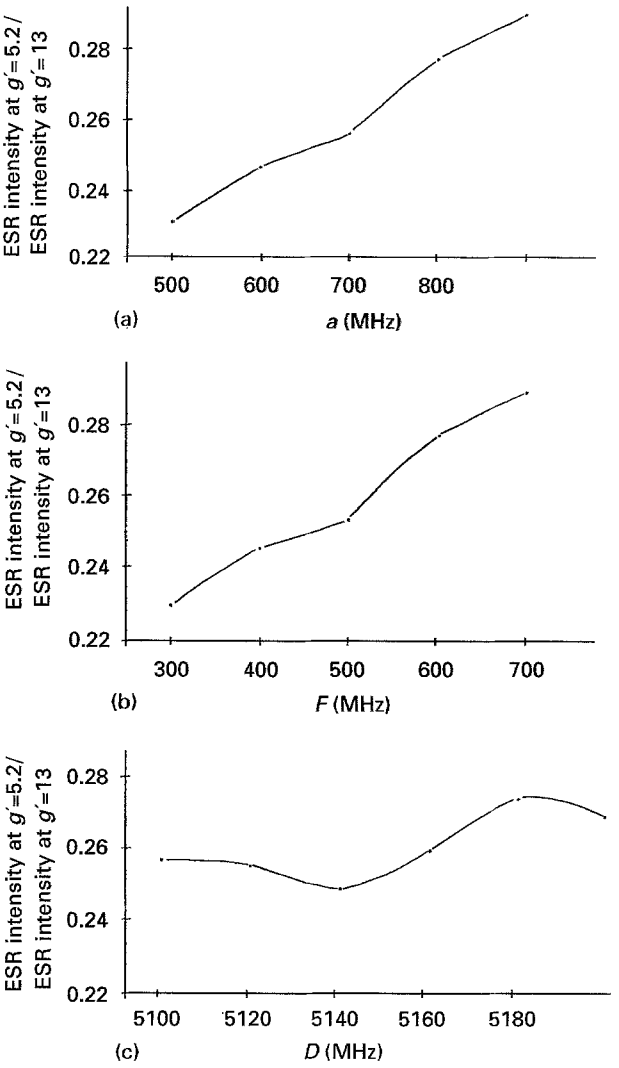

Figure 8 (a) Change of the intensity ratio of the two strong low-field signals at $g' \simeq 5.2$ and 13 as a function of the splitting constant a; (b) variation of F; (c) variation of D.

weaker. To prove this statement on a microscopic level, *in situ* ESR bending stress experiments were performed on glasses using different types of incorporated paramagnetic centres to monitor the reaction of the glassy matrix on the mechanical perturbation.

Changes in the local structure were indicated by a decrease of the ESR intensity of the transitions within the spin system of the paramagnetic probes. As Fig. 9 shows, distinct effects result for different radiation-induced paramagnetic defects (trapped holes like SiO^-/h^+ with $g > 2$ or trapped electrons M^{n+}/e^- with $g < 2$). Applying a linearly increasing load in the MPa range, a non-linear decrease of the signal amplitudes is caused by the superposition of different tension-induced line-broadening effects. The ESR response of the defects reflects not only the distortions of the local geometry and the perturbation of the electronic structure but also the changed orientation of the magnetic axes.

Coexisting trapped electron and hole centres in one and the same sample (Fig. 9; γ-irradiated, cadmium-containing sample) did react differently to the bending stress applied. This behaviour is caused by the different nature of the centres (e.g. depth of the traps) including their different interactions via spin–orbit coupling to the glassy network.

The response of the incorporated transition metal ions to bending stress applied in the ESR spectrometer is less pronounced (Fig. 10). The stress-induced changes do not reach those of the defects. To obtain measurable effects, ions with either a large g-anisotropy (Cu^{2+}) or with a large zero-field splitting (Cr^{3+}) were chosen. From an energetical point of view the two types of paramagnetic centres (i.e. the ions and the defects) represent deep and shallow impurity centres. Therefore, the reactions of the defects to the bending stress not only reflect the higher energy of their ground state but also their greater sensitivity to

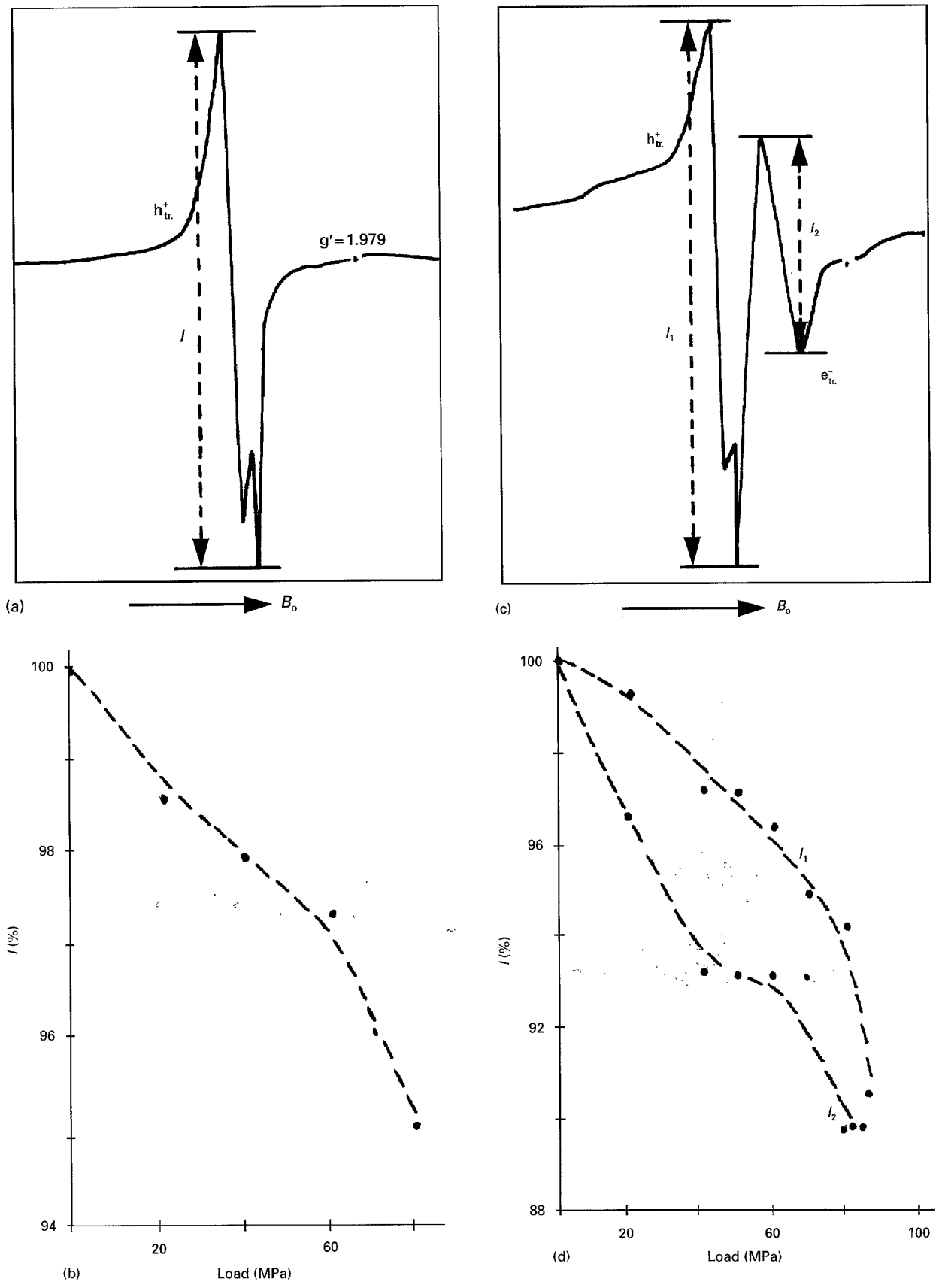

Figure 9 Influence of bending stress on trapped holes (h^+_{tr}) and electrons (e^-_{tr}) in γ-irradiated glasses: (a) h^+_{tr} in a glass of the composition 33 $CaO/6\ Al_2O_3/61\ SiO_2$ (mol %); (b) change of the signal intensity generated by application of bending load; (c) trapped h^+ and e^- centres in a glass of the composition 7.8 $CdO/21.4\ CaO/13\ Al_2O_3/57.8\ SiO_2$ (mol %); (d) intensity response on the effect of load of both centres.

structural changes such as the variation of bond angles at the formation of a stress state in the sample.

It should also be noted that the values of bending stress applied so far are insufficient to stimulate the recombination of defects.

4. Conclusion

Summarizing the observed phenomena one can establish the following advantages of the combination of a three-point bending stress arrangement with an ESR spectrometer: (i) direct and continuous observation of

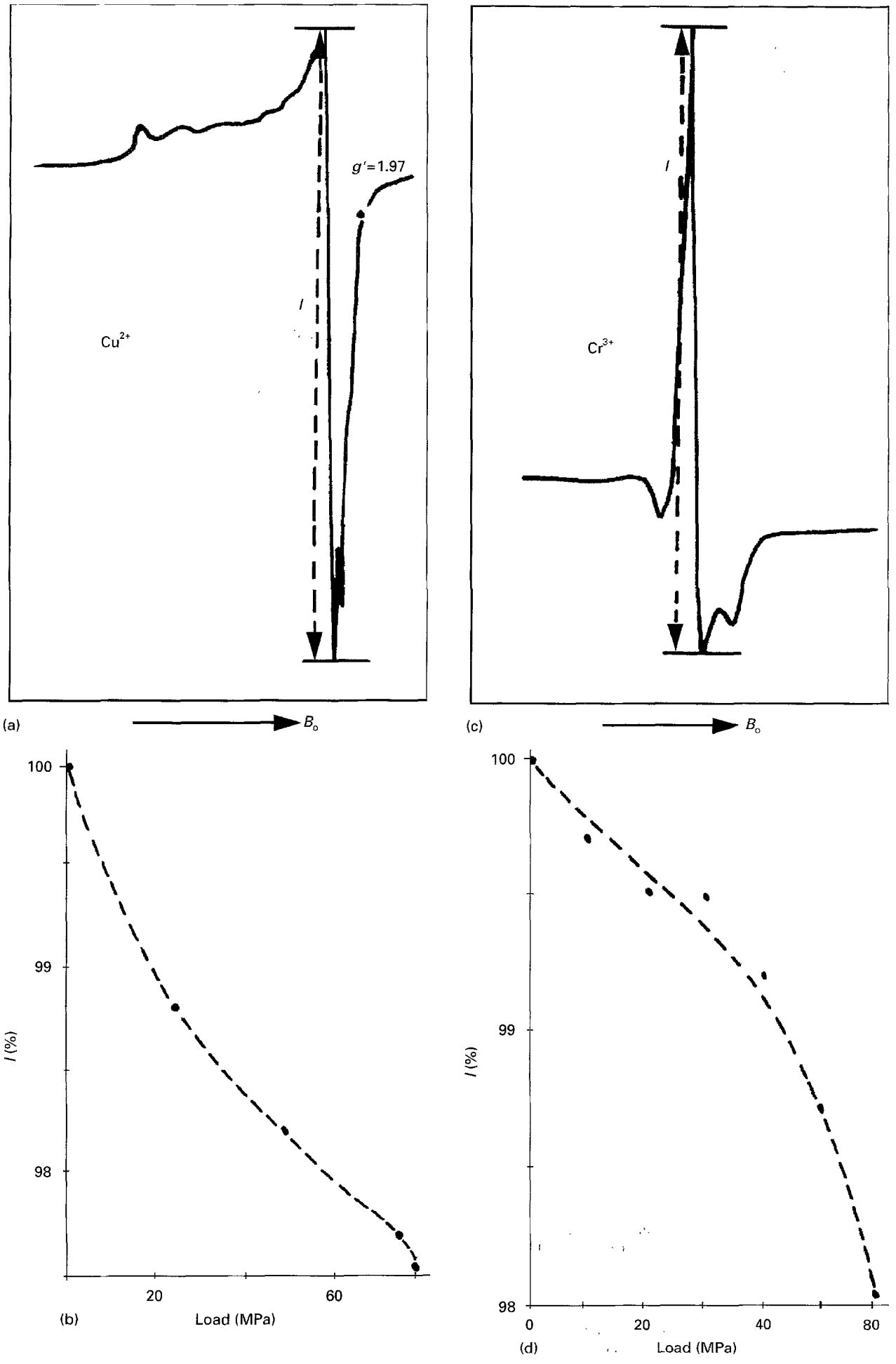

Figure 10 ESR intensity changes of the signals caused by (a) Cu^{2+} and (c) Cr^{3+} ions (0.1 mol/kg glass) containing glass samples of the composition (wt %) 61.5 SiO_2/9 ZrO_2/5 Al_2O_3/5 CaO/2.5 MgO/7 K_2O/10 Na_2O; (b) and (d) show the corresponding relative intensity changes.

the material under the action of bending stress up to mechanical destruction of the sample, (ii) optically transparent samples are not necessary, but a further direct combination with optical methods is, in general, possible, (iii) the high sensitivity and selectivity of the ESR method allow the first steps of stress influence on the local geometry to be followed long before the crack appears and fracture finally takes place, respectively, (iv) local effects are observed on the atomic scale which can be related to the mechanical properties by an appropriate hamiltonian, (v) the reversibility of the effects can easily be proved by a suitable alternating stress/relaxation regime, (vi) variation of further parameters, like temperature or application of tensile stress, is possible.

The combined bending stress experiments cannot only be used to indicate mechanically induced macroscopic processes competing with inner tensions in ceramic or glassy materials. They can also be used in a qualitative manner to identify paramagnetic species of different electronic structures and to support the assignments of the transitions between the corresponding spin states.

Acknowledgement

We thank the Deutsche Forschungsgemeinschaft for financially supporting these investigations.

References

1. R. STÖSSER, M. NOFZ, R. BRENNEIS, J. KLEIN and A. RERICHA, *Mater. Sci. Forum* **62–64** (1990) 279.
2. R. STÖSSER, J. KLEIN, M. NOFZ, R. LÜCK, A. RERICHA and R. BRENNEIS, *High Press. Res.* **7** (1991) 279.
3. M. NOFZ and R. STÖSSER, *Silikattechnik* **41** (1990) 310.
4. R. STOESSER, K. MAEDER, H.-H. BORCHERT and R. LUECK, *High Press. Res.* **13** (1994) 29.
5. R. STOESSER and R. BRENNEIS, *ibid.* **13** (1994) 71.
6. R. STÖSSER, R. BRENNEIS and I. EBERT, *J. Mater. Sci.* **25** (1990) 223.
7. R. S. DE BIASI and D. C. S. RODRIGUES, *ibid.* **2** (1983) 210.
8. V. BELTRAN-LOPEZ, J. CASTRO-TELLO, *J. Magn. Res.* **39** (1980) 437.
9. J. KLEIN, Thesis, Humboldt-University, Department of Chemistry, Berlin (1990).
10. R. STÖSSER, *High Press. Res.* **9** (1992) 259.
11. R. STÖSSER, R. BRENNEIS, W. HERRMANN and N. STEINFELDT, in "Hochleistungskeramik", edited by G. Petzow, F. Tobolski and R. Telle (VCH Verlagsgesellschaft m.b.H., Weinheim, 1995) pp. 281–97.
12. W. SCHULLE, in "Feuerfeste Werkstoffe" (Deutscher Verlag für Grundstoffindustrie m.b.H., Leipzig, 1990) pp. 68–79, 101–121 and 211–220.
13. R. LÜCK, R. STÖSSER and H. RAGER, *High Press. Res.* **7** (1991) 287.
14. R. BRENNEIS, R. STÖßER and W. HERRMANN, (unpublished data).

Received 6 February
and accepted 19 September 1995